Journal of Power Sources 245 (2014) 418–428

Contents lists available at SciVerse ScienceDirect

Journal of Power Sources

journal homepage: www.elsevier.com/locate/jpowsour

Effect of low temperature in-situ sintering on the impedance and the performance of intermediate temperature solid oxide fuel cell cathodes

Jimmi Nielsen*, Per Hjalmarsson, Martin Hangaard Hansen, Peter Blennow

Department of Energy Conversion and Storage, Technical University of Denmark, Frederiksborgvej 399, DK-4000, Denmark

HIGHLIGHTS

- LSC based cathodes are highly suitable for low temperature in-situ sintering.
- LSC based 800 °C in-situ sintered cathode showed an ASR of 0.05 Ω cm^2 at 650 °C.
- LSCF showed poor low temperature in-situ sintering capabilities.
- Poor cathode grain connectivity may distort the high frequency EIS response.
- Poor cathode adhesion may be detected by an additional EIS high frequency arc.

ARTICLE INFO

Article history:
Received 7 January 2013
Received in revised form
28 May 2013
Accepted 12 June 2013
Available online 5 July 2013

Keywords:
Cathodes
In-situ sintering
IT-SOFC
LSC
LSCF
Impedance

ABSTRACT

The effect of in-situ sintering temperature and time on the electronic conductivity, impedance and performance of IT-SOFC cathodes were studied. The studied cathodes were for comparison $(La_{0.6}Sr_{0.4})_{0.99}CoO_3$ (LSC), $(La_{0.6}Sr_{0.4})_{0.99}CoO_3$:$Ce_{0.9}Gd_{0.1}O_{1.95}$ (LSC:CGO), $La_{0.58}Sr_{0.4}Co_{0.2}Fe_{0.8}O_3$ (LSCF) and $La_{0.58}Sr_{0.4}Co_{0.2}Fe_{0.8}O_3$:$Ce_{0.9}Gd_{0.1}O_{1.95}$ (LSCF:CGO). The LSCF-based cathodes showed poor sintering capabilities compared to the LSC-based cathodes in the studied temperature range of 650–950 °C. The poor necking between individual LSCF grains lower the electronic conductivity. Furthermore, poor cathode/electrolyte adhesion was seen as an additional high frequency impedance arc, which gradually disappeared as the LSCF cathodes were sintered at increasing temperature. Effects on the impedance shape from poor cathode grain connectivity was shown through impedance simulations to result in a possible increase in the high frequency slope of the characteristic Gerischer impedance response of porous mixed ionic and electronically conducting (MIEC) cathodes. In contrast to LSCF, the LSC-based cathodes showed excellent sintering capabilities, electronic conductivity and performance. Scanning electron microscopy investigations showed that significant interaction already takes place at 750 °C between the LSC-based cathodes and the electrolyte. The polarization resistance (R_p) of the LSC based cathodes was 0.05 Ω cm^2, which to our knowledge is the best performance reported in the literature for a low temperature 800 °C in-situ sintered cathode.

1. Introduction

Solid oxide fuel cells (SOFCs) are promising electrochemical energy conversion devices due to high efficiency, fuel flexibility, low pollutant emissions and stack scalability. The last decade of research has to a large extent focused on lowering the SOFC operating temperature. This has some clear advantages, such as increased durability and the possibility of a significant wider choice of materials, which increases the chances of the SOFC technology to lower cost and become sufficiently competitive. The mixed ionic electronic conductors (MIEC) and composites with a good ionic conducting material, such as gadolinium doped ceria (CGO), is the common type of cathodes considered for 600–800 °C intermediate temperature SOFC (IT-SOFC). These types of cathodes are traditionally sintered above 1000 °C. In-situ cathode sintering offer a potential lowering of the cost since the high temperature cathode sintering step is avoided. Furthermore, the fabrication route of metal supported SOFCs (MS-SOFC) requires an in-situ cathode sintering below 900 °C due to corrosion [1]. Despite the extensive research in MIEC based cathodes very little is actually known about the effect of sintering temperature on the performance and thus

* Corresponding author. Tel.: +45 46775626.
E-mail address: jini@dtu.dk (J. Nielsen).

0378-7753/$ – see front matter © 2013 Elsevier B.V. All rights reserved.
http://dx.doi.org/10.1016/j.jpowsour.2013.06.067

impedance of MIEC-based cathodes. Some of the requirements for a low temperature in-situ sinterable cathode are:

- Good electrocatalytic activity
- Good electrical properties
- High sinterability
- Mechanical stability towards thermal cycling

The stability towards thermal cycling depends in practise on numerous parameters. As a first approximation it depends on matching of the Thermal Expansion Coefficients (TEC) of the various cell components. However, in practise an exact TEC match and a similar TEC temperature dependency of the various components is not possible. Temperature gradients will also always be present, which induces stresses. Furthermore, the adhesion of the cathode to the electrolyte, the thickness of the cathode, and the temperature history and range of operation also affects the mechanical robustness of the cathode. Nevertheless, all requirements mentioned above must be fulfilled for a successful in-situ sintered cathode.

A few studies have demonstrated that in-situ and low temperature sintering of various potential SOFC cathodes such as $La_{0.6}Sr_{0.4}Co_{0.2}Fe_{0.8}O_{3-\delta}$ (LSCF), $Sm_{0.5}Sr_{0.5}CoO_3$:$Sm_{0.2}Ce_{0.8}O_{1.9}$ (SSC:SDC), $SmBa_{0.5}Sr_{0.5}Co_2O_{5-\delta}$:$Ce_{0.9}Gd_{0.1}O_{1.9}$ (SBSC:CGO) and $Ba_{0.5}Sr_{0.5}Co_{0.8}Fe_{0.2}O_{3-\delta}$ (BSCF) is feasible on button cell level [2–5]. Baek et al. compared the properties of in-situ sintered SBSC:CGO and BSCF cathodes with conventional cathodes such as $La_{0.8}Sr_{0.2}MnO_{3-\delta}$ (LSM82), $La_{0.8}Sr_{0.2}FeO_{3-\delta}$ (LSF82), LSCF and SSC:SDC [5]. Despite these studies the knowledge is sparse about the implication of poor connectivity of the cathode grains and poor cathode/electrolyte adhesion on the electrical conductivity, the serial resistance, the electrochemical performance, and hence the impedance response of low temperature in-situ sintered cathodes.

The focus of the present study is to systematically study the effect of low temperature in-situ sintering on the performance and the impedance response of MIEC and MIEC:CGO composite cathodes in the temperature range 650–950 °C. The MIEC materials and MIEC:CGO composites studied are $La_{0.58}Sr_{0.4}Co_{0.2}Fe_{0.8}O_3$, $La_{0.58}Sr_{0.4}Co_{0.2}Fe_{0.8}O_3$:$Ce_{0.9}Gd_{0.1}O_{1.95}$, $(La_{0.6}Sr_{0.4})_{0.99}CoO_3$ and $(La_{0.6}Sr_{0.4})_{0.99}CoO_3$:$Ce_{0.9}Gd_{0.1}O_{1.95}$. Of convenience, these compositions will in the following be referred to as LSCF, LSCF:CGO, LSC and LSC:CGO. These material combinations are expected to have different properties such as sinterability, electronic and ionic conductivity, which consequently should be reflected in the performance. Thus, a comparison of these cathodes is expected to shed further light on the importance of these properties.

2. Theory

The porous structure of the MIEC based cathodes can be modelled as columns as illustrated in Fig. 1 [6,7]. Each column can be described by the general transmission line depicted in Fig. 1 with the following general solution [8–11]:

$$Z = \frac{\chi_1\chi_2}{\chi_1+\chi_2}\left(L + \frac{2\lambda}{\sinh(L/\lambda)}\right) + \lambda\frac{\chi_1^2+\chi_2^2}{\chi_1+\chi_2}\coth\left(\frac{L}{\lambda}\right) \quad (1)$$

with

$$\lambda = \sqrt{\frac{\zeta}{\chi_1+\chi_2}} \quad (2)$$

Here L is the thickness of the electrode and λ is the characteristic AC penetration length or equivalent the electrochemical utilization thickness of the electrode. Eq. (1) represents the impedance (in Ω) of a single column shown in Fig. 1, but in principle the porous

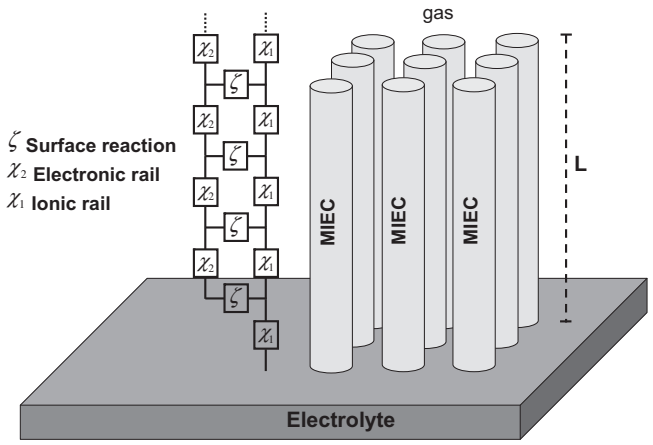

Fig. 1. The porous MIEC electrode is modelled as columns, which can be described by the general transmission line.

electrode consists of n columns pr. area. However, it is difficult to determine the exact number of columns pr. area in the porous electrode. A much easier and equivalently informative approach is to consider the porous electrode effectively as one column pr. area. This enables a direct application of Eq. (1). For the case where the cathode grains are sintered well together, the well known Gerischer response can be obtained by making the reasonable assumption that the electronic conductivity is significantly higher than the ionic conductivity $\chi_2 << \chi_1$, which results in Eq. (1) being simplified to:

$$Z = \lambda\chi_1\coth\left(\frac{L}{\lambda}\right), \text{ with } \lambda = \sqrt{\frac{\zeta}{\chi_1}} \quad (3)$$

The transport of oxide ions via diffusion in the MIEC column can be modelled as a resistor pr. unit length (in Ω cm^{-1}):

$$\chi_1 = r_{gi} \quad (4)$$

Finally the impedance of the surface reaction ζ (in Ω cm) can be modelled as a simple parallel combination between a resistor r_r and a constant phase element q_r (CPE):

$$\zeta = \frac{r_r}{1 + r_r q_r (j\omega)^{\alpha_r}} \quad (5)$$

The unit of the impedance ζ is Ω cm because it is the area specific impedance of the column surface (in Ω cm^2) divided by the perimeter of the column. For thick cathodes $L >> \lambda$ and coth $(L/\lambda) \rightarrow 1$, which implies, that the Gerischer impedance response has the shape of a skewed semicircle. The expression originating from Eq. (3) with the assumptions in Eq. (4) and Eq. (5) is in accordance with the following Finite-Length-Gerischer (FLG) expression derived in Ref. [6]:

$$Z = \frac{RT}{4F^2C_V^0}\sqrt{\frac{A}{D_V^{\text{eff}}k_0}}\,\frac{\coth\left((L/\lambda_0)\sqrt{1+j\omega/k_o}\right)}{\sqrt{1+j\omega/k_o}}, \quad \text{with } \lambda_0 = \sqrt{\frac{AD_V^{\text{eff}}}{k_0}} \quad (6)$$

R is the gas constant, T is the temperature, F is faradays constant, C_V^0 is the concentration of oxygen vacancies, A is the thermodynamic enhancement factor, D_V^{eff} is the effective oxygen vacancy diffusion coefficient, k_0 is the surface reaction rate constant and L is the thickness of cathode. For further explanation the reader is referred

to [6]. Comparison of the expressions provides a physical interpretation of the involved resistances and capacitive elements in Eqs. (4) and (5). Improper necking between individual cathode grains is expected to result in a deviation from the Gerischer response.

3. Experimental

3.1. Symmetrical cell preparation

The materials used in the present study to prepare screen printing pastes were $Ce_{0.9}Gd_{0.1}O_{1.9}$ (Fuel Cell Materials, USA), $(La_{0.6}Sr_{0.4})_{0.99}CoO_3$ (in house made) and $La_{0.58}Sr_{0.4}Co_{0.2}Fe_{0.8}O_3$ (Seimi, Japan). The particle size distributions of the powders (LSCF, LSC and LSC:CGO) as determined by laser diffraction were similar with d_{10}'s of 0.2–0.3 μm, d_{90}'s of 1.6–2.0 μm and d_{50}'s of 0.4, 1.1 and 1.1 μm, respectively. The prepared pastes for LSC:CGO and LSCF:CGO composite cathodes contained a mixture of 50:50 wt. % either LSC or LSCF and CGO. The pastes were prepared by mixing raw powders with a solvent, a binder and a surfactant. All three cathodes were shaped by screen printing an approximately 30 μm thick layer onto both sides of a 200 μm ± 20 μm or a 300 μm ± 30 μm thick and 50 × 50 mm^2 large, commercial densely sintered CGO tape (Kerafol, Germany). These cells, containing green ceramic layers, were laser cut to 6 × 6 mm^2 samples and later used in the symmetrical cell tests.

3.2. Electrochemical impedance measurements

The 6 × 6 mm^2 symmetrical cells with unsintered cathodes were applied with Pt Paste to form a current collecting layer. The cells were hereafter sandwiched in between fine-meshed Pt nets in the test setup. The measurements were conducted in specially designed rigs, which have been constructed to allow simultaneous testing of four symmetric cells per test run, with fully automated changes of testing conditions, such as temperature and gas composition. The cells were characterized by electrochemical impedance spectroscopy (EIS) at open circuit voltage (OCV) in air in the temperature range 650–950 °C. The EIS spectra were preferentially obtained using a Solartron 1260 FRA in the frequency range 1 MHz–1 Hz. However, in some cases a Hioki impedance analyzer was used with EIS acquisition in the frequency range 100 kHz–1 Hz. For all cases the EIS perturbation amplitude was 30 mV RMS. The acquired EIS data were corrected for inductance from wires etc. by subtracting an EIS spectrum of the test setup without any cells. The impedance data were analyzed in a MatLab laboratory developed program with equivalent circuit model fitting using the complex non-linear least square (CNLS) fitting routine.

3.3. In-plane cathode electrical conductivity measurements

53 × 53 mm^2 large state of the art ceramic SOFCs, onto which a CGO interdiffusion barrier layer had been applied, were screen printed with the above described pastes in Section 3.1. The printed area was 40 × 40 mm^2. These samples were used for in-plane DC conductivity measurements. The in-plane conductivity was studied using the van der Pauw technique [12]. The resistance between the four corners of the prints was systematically measured using a Keithley 2700 multimeter. The methodology for calculating the in-plane conductivity is described elsewhere [13].

3.4. Microstructural characterization

The cathode/electrolyte interaction, and thus adhesion of the low temperature sintered cathodes with the electrolyte, was investigated by dissolving the cathodes in a 3 vol. % hydrochloric acid solution. The former cathode/electrolyte interfaces were hereafter studied by scanning electron microscopy (SEM). The microstructure of polished cross-sections of the symmetrical cell samples were also characterised by SEM. These samples were prepared by vacuum embedding the samples in Struers epoxy resin (Epofix); ground using SiC paper; polished using 6, 3 and 1 μm diamond paste, and then carbon coated to eliminate surface charging. The samples were observed using a Zeiss Supra 35 equipped with a field emission gun (FEG).

4. Results and discussion

4.1. Electronic conductivity as a function of sintering temperature and time

In Fig. 2A the in-plane electrical conductivity during in-situ sintering at approximately 850 °C is shown as a function of time for LSCF, LSC and LSC:CGO cathodes. Comparison shows that LSC by far exhibits the highest conductivity with a value around 260 S cm^{-1}. Mixing LSC with equal amounts (wt.%) of CGO lowers the cathode conductivity to around 65 S cm^{-1}, which is approximately one quarter the value of the pure LSC cathode. The lowest electrical conductivity is seen for the LSCF cathode with a value around 16 S cm^{-1}. For comparison typical bulk conductivities measured on dense samples at 850 °C have been determined to be around 1800 S cm^{-1} for LSC [14] and around 270 S cm^{-1} for LSCF [15,16]. Thus, the introduction of porosity and potentially an effect from low temperature sintering, lower the conductivities considerably. The electrical conductivities can be approximated as the electronic conductivities of the materials since their bulk ionic conductivity of less than 100 mS cm^{-1} is insignificant in comparison to the electronic counterpart [17,18]. In the experimental setup used in this study, Pt paste and Pt nets assures a high density of contact points and therefore insignificant constriction on current collection. However, in practical stack systems this may not be the case and usually an extra current collecting layer (CCL) is applied to ensure sufficient electrical contact and spreading of the electrochemical reaction. Thus, the contacting depends on the combination of the electronic conductivity of the cathode and the current collecting layer and the density of contact points. The better electronic conductivity of the cathode the less demanding is the cell contacting. The impact on conductivity of in-situ sintering temperature and development with time for LSCF is shown in Fig. 2B. Firstly, it is possible to see a clear effect of sintering temperature. The question is of cause whether the increase in conductivity is a consequence of further cathode sintering or a consequence of an increase in temperature. It is reported within the literature that the conductivity of LSCF with the stoichiometry in question increases with increasing temperature up to approximately 550 °C, which can be accounted for according to the small polaron hopping mechanism. Above approximately 550 °C the conductivity decreases with increasing temperature, which is argued to be related with the loss of oxygen and thus the formation of oxygen vacancies. For further details on these aspects the reader is referred to [15,16]. Thus, the temperature dependency of the conductivity is a unique fingerprint for the LSCF material. In Fig. 3 the cooling curves are shown for the 800 °C, 857 °C and 900 °C sintered LSCF cathodes in Fig. 2B. A similar trend for the 857 °C and 900 °C sintered LSCF cathodes is observed as in the above mentioned literature with a maximum in the conductivity as a function of temperature. However, the conductivity maximum of the in-situ sintered cathodes in Fig. 3 occurs at the value around 750 °C and not at the literature value of 550 °C. For the cathode sintered at the lowest temperature of 800 °C a maximum in conductivity is completely absent. These observations indicate that the necking of the individual cathode grains influence the electrical conductivity to a large extent. In

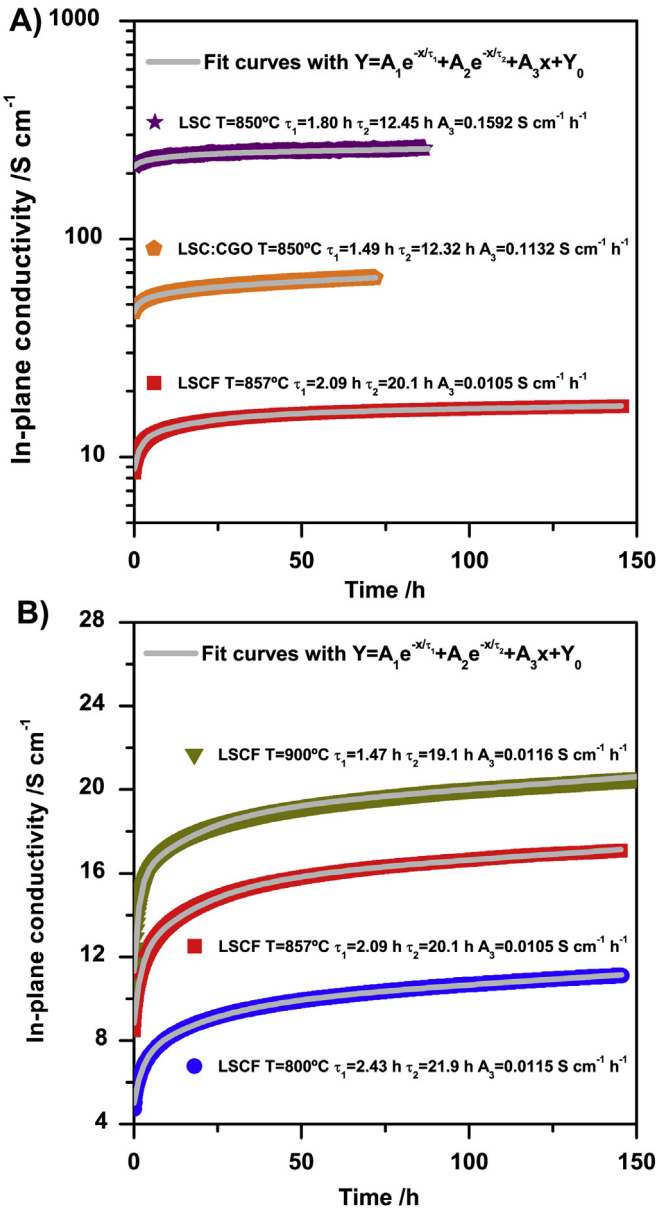

Fig. 2. The effect of in-situ sintering temperature and time on the in-plane electrical conductivity of LSC, LSC:CGO and LSCF cathodes. A) Conductivity of the different cathodes in-situ sintered at 850 °C. B) Effect of the in-situ sintering temperature on the conductivity of LSCF cathodes.

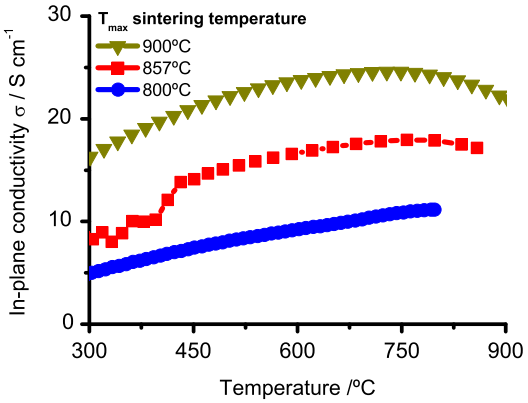

Fig. 3. Cooling curve showing the effect of temperature on the electrical conductivity of the LSCF long term sintered cathode presented in Fig. 2B.

other words the cathode particles are poorly interconnected due to insufficient sintering. In such cases the electrons may be transferred from one grain to the other via a conduction hopping mechanism and an Arrhenius like temperature dependency of the electronic conductivity is expected. This has been observed and described in details for ceramic contacts, where activation energies in the range from 10 to 30 kJ mol^{-1} were observed [19,20]. Calculation of the corresponding conductivity activation energies from Arrhenius plots of the data in Fig. 3 provide activation energies ranging from 5 to15 kJ mol^{-1}, which is in agreement with the bulk conductivity polaron activations energies reported in the literature [15,16]. Thus, the LSCF bulk electrical conductivity cannot be distinguished from the grain boundary electrical conductivity by the activation energies as the associated activation energy for the different conduction mechanisms is similar in magnitude.

Nonetheless, the results of Fig. 2 are a true improvement in conductivity and not an effect of temperature. The cause of the improvement must be better connectivity between the individual cathode grains. Beside increased conductivity with increasing sintering temperature it is also possible to see an improvement in conductivity with time, where an apparent ongoing linear increase in the conductivity is seen even after 150 h. Lowering the temperature in such isothermal conductivity experiments stops the apparent long term increase in the conductivity. This is illustrated by the experiment shown in Fig. 4. Thus, the ongoing changes in conductivity after more than hundred hours seem to be a true improvement in the conductivity of the cathode. From the data in Fig. 4 it is clear that the mechanism resulting in the long term conductivity improvement is a thermal activated process. This indicates, that the apparent ongoing long term conductivity improvement is a further sintering and thereby improvement of the necking between the individual cathode grains.

For characterization purposes only, the in-situ conductivity data in Fig. 2 has been fitted with an expression consisting of two exponential functions and a linear term. It was found that at least two exponential functions were needed in order to describe the initial evolution in conductivity, whereas a linear term satisfactorily describes the long term development. Each exponential function in the fitting equation represents a first order process with a characteristic time constant τ. The sintering process is presumably rather complex with different sintering mechanisms dominating at different stages of the sintering. Whether the fitted expression reflects the different sintering mechanisms is difficult to say and beyond the scope of the present study. Nonetheless, it does provide

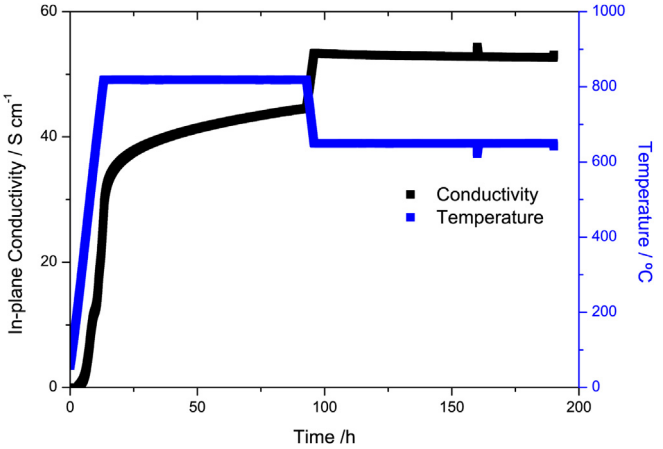

Fig. 4. The effect on conductivity evolution of a sudden lowering of the sintering temperature for an LSC:CGO cathode.

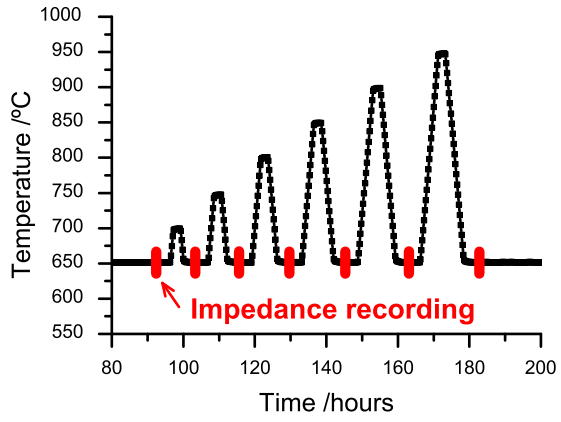

Fig. 5. Temperature profile for systematically studying the impact of sintering on EIS of LSC, LSC:CGO, LSCF, LSCF:CGO cathodes.

some numbers and characteristic time scales for the in-situ cathode sintering.

4.2. Impedance as a function of sintering temperature

For studying of the impact of sintering on the performance and the impedance response of MIEC cathodes and MIEC:CGO composite cathodes an approach illustrated by the temperature profile shown in Fig. 5 was used, where a gradual increase in sintering was characterized by impedance spectroscopy. The symmetrical cells with unsintered cathodes were initially ramped to 650 °C. Hereafter the symmetrical cells experienced a gradual 50 °C higher maximum temperature T_{max} with a dwell time of 2 h at T_{max} according to the temperature profile in Fig. 5. For the case of LSC and LSCF:CGO cathodes the initial T_{max} sintering temperature was 700 °C and 750 °C respectively. An impedance spectrum was recorded at 650 °C after each increment in T_{max} as indicated with red marks in the temperature profile of Fig. 5. Each row in Fig. 6 shows the impedance plots at 650 °C measured according to Fig. 5. Every test with a given type of cathode contained 4 samples, which all showed the same trend as depicted in Fig. 6. Generally it is possible to see a gradual change in the shape of the impedance spectra as T_{max} is increased. With increasing T_{max} the impedance shape goes towards that of the Gerischer impedance response, which is expected for well sintered cathodes with good interconnectivity between the cathode grains [6]. For the spectra that have experienced a T_{max} of 900 °C and/or 950 °C it is possible to obtain relatively good fits with a Gerischer impedance response as shown in Fig. 6. In the fitting, a Finite-Length-Warburg (FLW) impedance response has been used to account for the oxygen gas diffusion observed at low frequencies for the well performing LSCF:CGO, LSC and LSC:CGO cathodes. This is justified in Section 4.4, where the gas diffusion impedance is resolved. In addition to the Gerischer and the oxygen gas diffusion impedance responses a

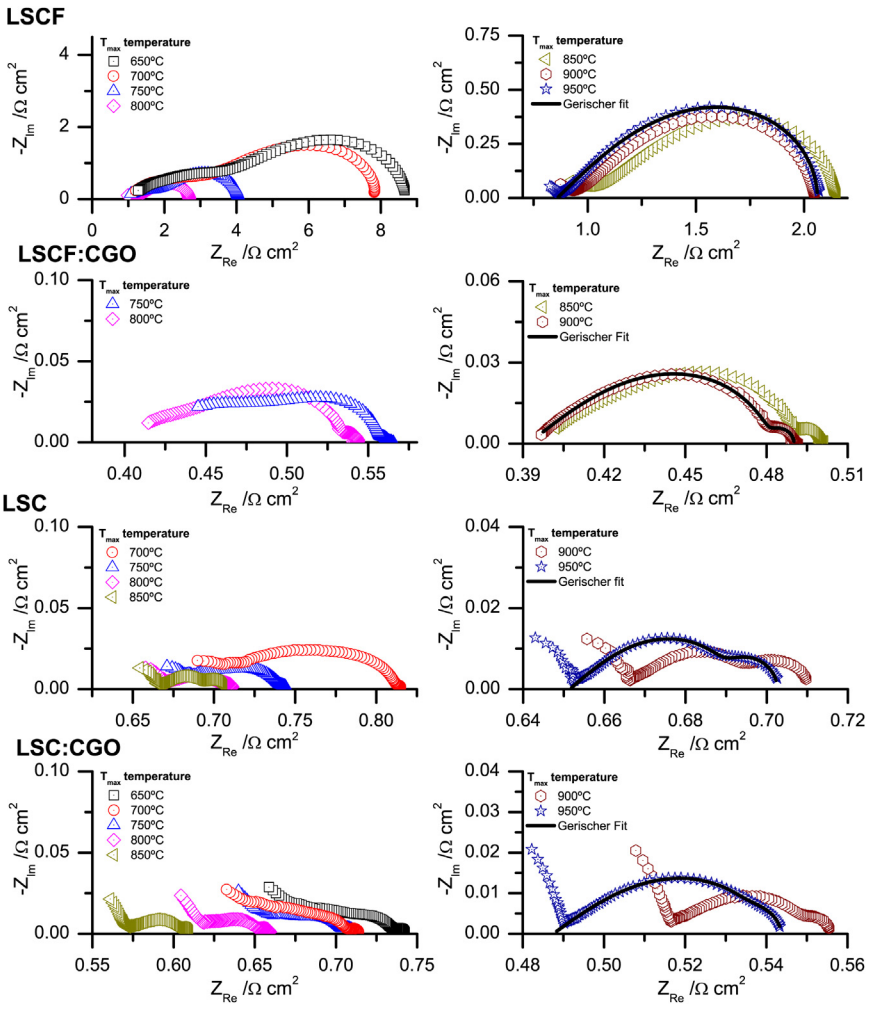

Fig. 6. Impedance of LSC, LSC:CGO, LSCF, LSCF:CGO cathodes as a function of the maximum sintering temperature T_{max}.

partly resolved arc at high frequencies is observable for the LSCF, LSC and LSC:CGO cathodes in Fig. 6. The Gerischer impedance response describes the response from the porous cathode, which means that the additional arc must be due to a process taking place before the Gerischer EIS response of the porous electrode. Thus, the arc is limited to either originating from the grain boundaries within the polycrystalline electrolyte or the cathode/electrolyte interface. For the spectra of the cathodes sintered at the lowest T_{max} the different responses overlap. The lower T_{max} the stronger is the merging of the various impedance contributions and a significant contribution from the connectivity of the individual grains within the cathode itself can in principal no longer be excluded. In Section 4.1 it was argued that the electronic conductivity is orders of magnitude better than the ionic conductivity. It implies that the prerequisite $\chi_2 << \chi_1$ for Eq. (3) is fulfilled. That the LSCF cathodes are not limited by the electronic conductivity is also indicated by comparison with the LSCF:CGO cathodes. Introduction of CGO in the cathodes lowers the electronic conductivity, however the result is not an increase in polarisation resistance. Instead a significant decrease is observed. This is ascribed to the significant improvement in the ionic conductivity as a result of the introduced CGO network. Similar performance has been obtained for a 900 °C sintered LSCF:CGO in Ref. [6]. Hence, Eq. (3) is valid and it is therefore only the oxide ion transfer across cathode grain boundaries which may add to the impedance given by Eq. (3). Such an impedance contribution from the grain boundaries within the cathode would imply that the diffusion of oxide ions no longer can be represented as a resistor pr. unit length as in Eq. (4). One possible way of modelling the situation is to replace Eq. (4) with the following expression describing a resistor r_{gi} in series with a parallel combination with a resistor r_{gb} and a CPE q_{gb}:

$$\chi_1 = r_{gi} + \frac{r_{gb}}{1 + r_{gb} q_{gb} (j\omega)^{\alpha_{gb}}} \quad (7)$$

r_{gi} is a resistor associated with the transport of oxide ions in the grain interior of the individual cathode grains, while the parallel combination of a resistor r_{gb} and a CPE q_{gb}, represents the oxide ion transport across the individual grain boundaries within the cathode. Fig. 7 shows three different transmission line responses. The first describes a coupling between a resistor and a capacitor yielding a 45° slope in a Nyquist plot. In the second transmission line a resistor has been added in parallel with the capacitor. The resulting impedance response is a skewed semicircle, which can represent the ideal Gerischer response [21] or the ideal classical porous electrode theory response originally derived by de Levie [22]. It is referred to as ideal since a capacitor and not a CPE is involved in the transmission line. The name of the characteristic skewed semicircle response depends on the nature of the ionic transport process involved. If the transport process is diffusion then it should be referred to as a Gerischer whereas if the transport process is conduction it should be named porous electrode theory response. The third transmission line response represents the MIEC Gerischer impedance response of the present study, where the possibility of an effect from poor cathode grain–grain connectivity according to Eq. (7) has been included. Since the ideal response of a capacitor is rarely seen in practical measurements, the capacitors have been replaced with CPE elements. Possible impedance shapes of the third transmission line response in Fig. 7 are shown in Fig. 8. Starting with the unrealistic case of a very high q_{gb} value the impedance shape of the solid black line of Fig. 8A is acquired. At the high frequency end a skewed semicircle is observed due to the coupling between r_{gi} and the parallel coupling between r_r and q_r.

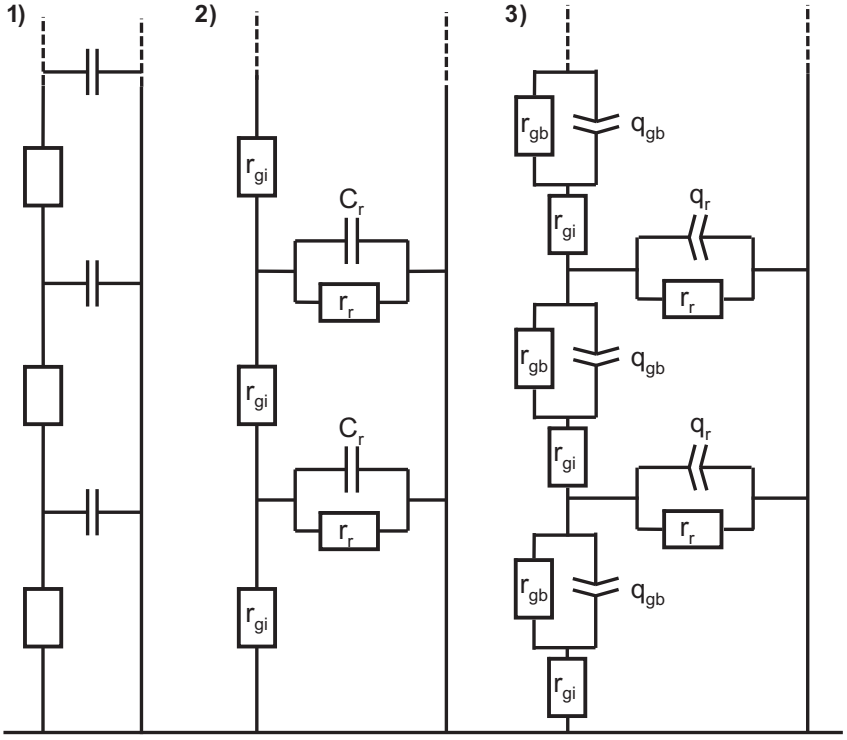

Fig. 7. 1) Transmission line representing a porous MIEC cathode without a surface reaction. 2) Transmission line representing a porous MIEC electrode with a surface reaction, which normally is referred to as a Gerischer impedance response. 3) Modified Gerischer impedance response, where the effect of poor cathode grain–grain connectivity has been taken into account.

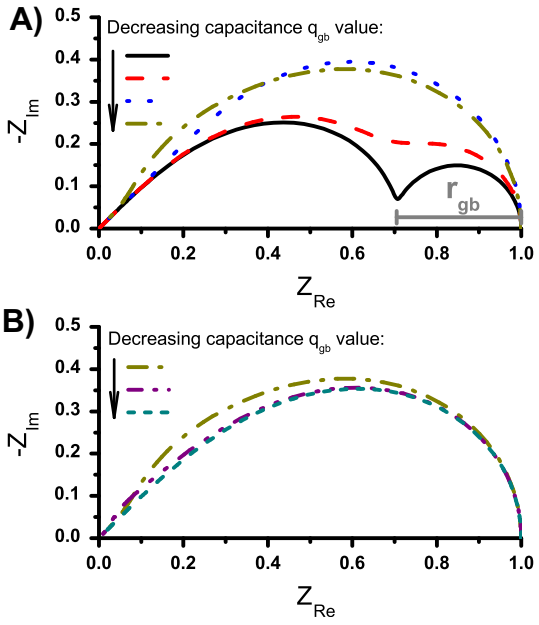

Fig. 8. Possible impedance responses of the third transmission line presented in Fig. 7.

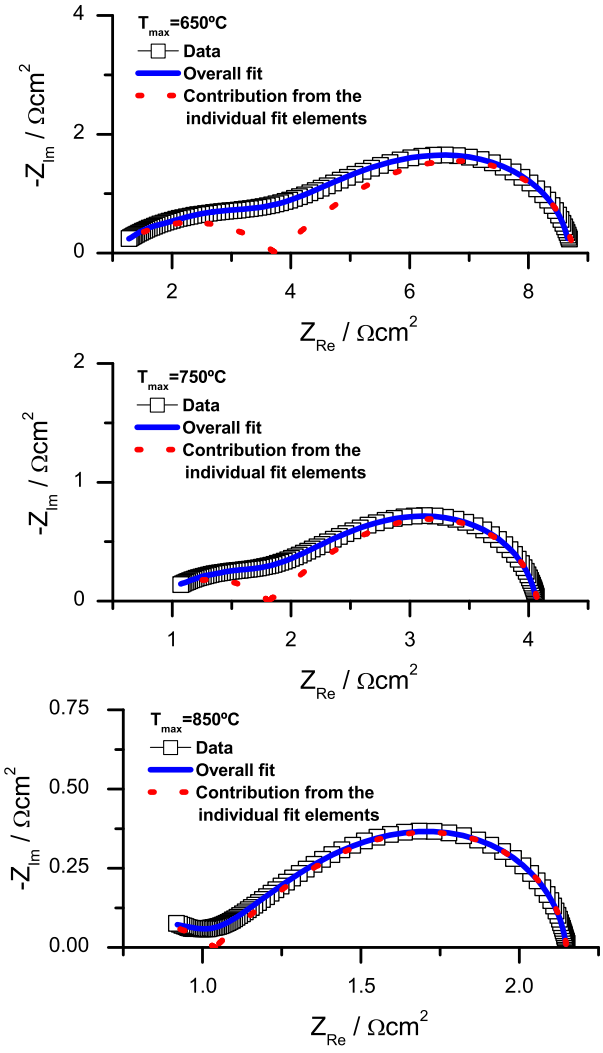

Fig. 9. Impedance fits with the equivalent circuit $R_s(R_{hf}Q_{hf})G$ of the LSCF impedance spectra in Fig. 6, where G represents the Gerischer EIS response.

This is followed by the semicircle response from the parallel coupling between r_{gb} and q_{gb}. As the value of q_{gb} is continuously decreased the semicircle of the r_{gb} and q_{gb} coupling moves towards higher frequencies and merges together with the skewed semicircle response as illustrated in Fig. 8A and B. It is clear that the opposite case of the situation represented by the solid black line in Fig. 8A cannot occur with the ($r_{gb}q_{gb}$) suppressed semicircle appearing before the Gerischer response. The ideal high frequency 45° slope of the Gerischer response reflects the electrochemical extension from the cathode/electrolyte interface out into the porous electrode. It is obvious that a response from the cathode grain boundaries cannot occur before they are electrochemically active. Thus, the possible realistic effect from cathode grain boundaries seems to be a distortion of the Gerischer high frequency end, which may give rise to a slope larger than the characteristic 45° of the ideal Gerischer impedance response. The appearance of a high frequency arc in e.g. the LSCF spectra of Fig. 6 can therefore not originate from the cathode grain boundaries. Nor can it originate from the electrolyte grain boundaries since such a contribution from the high temperature sintered electrolyte would be constant in the studied temperature range and not evolve as in Fig. 6. The main part of the high frequency contribution must therefore necessarily originate from the cathode/electrolyte interface with the cathode adhesion being improved as the sintering temperature T_{max} is increased. This implies that an impedance model of a serial combination of a suppressed semicircle (RQ) and a Gerischer impedance response should be able to account for the LSCF spectra. A few representative fits at different temperatures are given in Fig. 9, which reveals that the high frequency (RQ) arc needs to be severely suppressed with an exponent as low as 0.45 for the spectra with the lowest T_{max} sintering temperature. The exponent α_r in Eq. (5) for the Gerischer element varied in between 0.9 and 1 in the fitting of the LSCF spectra. Even though a CPE with an exponent as low as 0.45 seems physical unrealistic the impedance model can nonetheless provide good fits of all the LSCF spectra with different T_{max} sintering temperatures in Fig. 6. In principle the modified Gerischer represented by the third transmission line in Fig. 7, which takes grain boundaries into account, should be used in the fitting. However, the modified Gerischer is only able to affect the high frequency part of the Gerischer impedance as discussion earlier and will therefore not significantly affect the severely suppressed semicircle (RQ). Taking the strong overlap of the impedance elements of the low T_{max} sintered spectra into consideration it makes little sense to add further variables into the model. It is inherently difficult to justify and account for all dispersion effects in a low temperature sintered cathode, which barely sticks together. Furthermore, the basis for the whole transmission line approach is that the situation can be treated as an one dimensional problem. In practise, it means that the extension of the electrochemical reaction λ is many times larger than the size δ of the grains constituting the cathode $\lambda >> \delta$. Whether this condition is fulfilled for the spectra of the lowest T_{max} sintering temperatures is difficult to say. The poor adhesion and necking between the grains will limit the electrochemical extension.

In contrast, the partly resolved high frequency arcs in the spectra of the LSC and the LSC:CGO electrodes in Fig. 6 must necessarily be related to grain boundaries within the electrolyte since the impedance contribution from these arcs are relatively unaffected by the change in cathode sintering temperature T_{max}. In the spectra of the LSCF electrode sintered at a T_{max} at or above 850 °C it is also possible to see the onset of a relatively small arc that is independent of T_{max}, which could be the response from the

electrolyte grain boundaries. The spectra of the LSCF:CGO cathode are limited to 100 kHz unlike the remaining spectra of Fig. 6, which are recorded with a maximum frequency of 1 MHz. Furthermore, for the symmetrical cells with LSCF:CGO cathodes a 185 μm thick tape was used, while for the remaining symmetrical cells, tapes with a thickness of 300 μm ± 30 μm was used. The thinner electrolyte tape and the limited maximum frequency of 100 kHz explains why no response from the electrolyte grain boundaries is observed for the symmetrical cells with LSCF:CGO cathodes. Thus, the serial resistance R_s is interpreted as the high frequency interception with the real axis of the Gerischer response. Taking the variation of the electrolyte tapes into account, the serial resistance R_s of all the different cathodes in Fig. 6 is of the same magnitude except for LSCF, which shows a somewhat higher value. In order to acquire knowledge on the adhesion and thus the interaction at the cathode/electrolyte interface, low temperature sintering experiments were carried out in a furnace of the different cathodes. The cathodes were after the low temperature sintering removed by dissolution in a 3 vol. % hydrochloric acid solution after which the former cathode/electrolyte interface was examined by SEM. Fig. 10 shows the results for LSCF and LSC:CGO cathodes sintered at 750 °C and 850 °C for 4 h. From the micrographs it can be seen that significant interaction has taken place, also at 750 °C, between the LSC:CGO cathode and the CGO electrolyte as evidenced by a relatively high concentration of 20–100 nm sized crater like structures on the electrolyte surface. These craters form the remaining imprints of the cathode grains after their removal. Similar crater like structures have also been observed previously for well sintered LSM:YSZ cathode YSZ electrolyte interfaces [23] and is an indication of sufficient and good adhesion. In contrast to the LSC:CGO cathode it is not possible to see any crater like structures on the electrolyte surface for the LSCF cathode after sintering at 750 °C. After sintering LSCF at 850 °C some crater like structures starts to appear on the electrolyte surface. However, the density of crater like structures are significant less and not as pronounced as in the case of LSC based cathodes. These differences may explain and support the interpretation made earlier on. The low density of crater like structures for LSCF compared to LSC:CGO in Fig. 10 explains the higher R_s of the LSCF spectra. Furthermore, the observed absence of crates after sintering at 750 °C for LSCF support the interpretation, that the high frequency arc in the LSCF spectra, which disappears with increasing T_{max}, is a response due to poor adhesion between the LSCF cathode and the CGO electrolyte. Fig. 11 shows cross sections of a LSCF and a LSC cathode sintered at 950 °C for 2 h. The micrographs show the LSCF cathode to be very grainy with poor necking between the individual cathode grains. In contrast, the LSC cathode shows excellent necking.

4.3. Cathode performance as a function of sintering temperature

Performance wise it is expectable that the serial resistance R_s will depend on the electronic conductivity of the cathode, the current constriction at the cathode/electrolyte interface and the ionic conductivity of the electrolyte. Thus, an increase in sintering temperature T_{max} will only have a beneficial effect on R_s and any effects from poor connectivity due to improper sintering. For the case of the Gerischer polarization resistance R_p we have a situation where R_p is co-limited by the MIEC bulk oxide ion diffusion (r_{gi} in

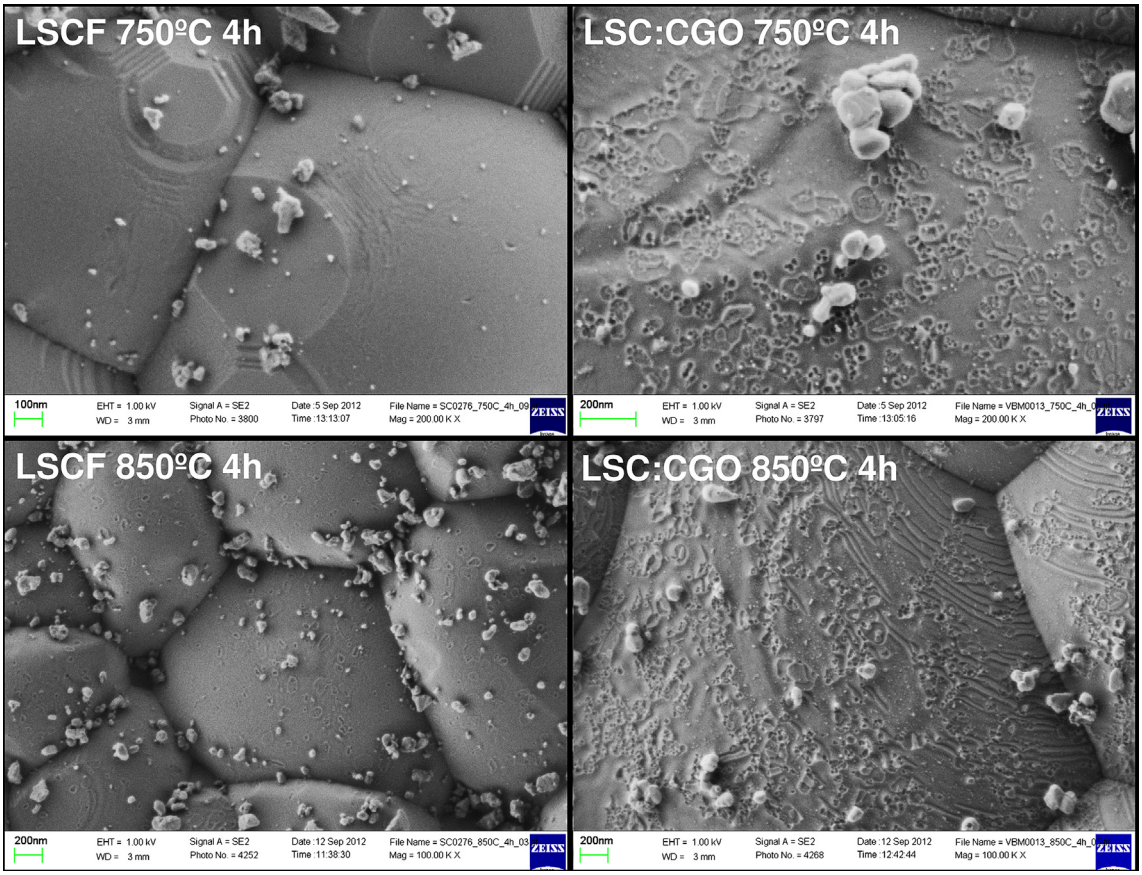

Fig. 10. The cathode/electrolyte interface of LSCF and LSC:CGO cathodes sintered at different temperatures for 4 h. The cathode has been removed by dissolution in a hydrochloric acid solution.

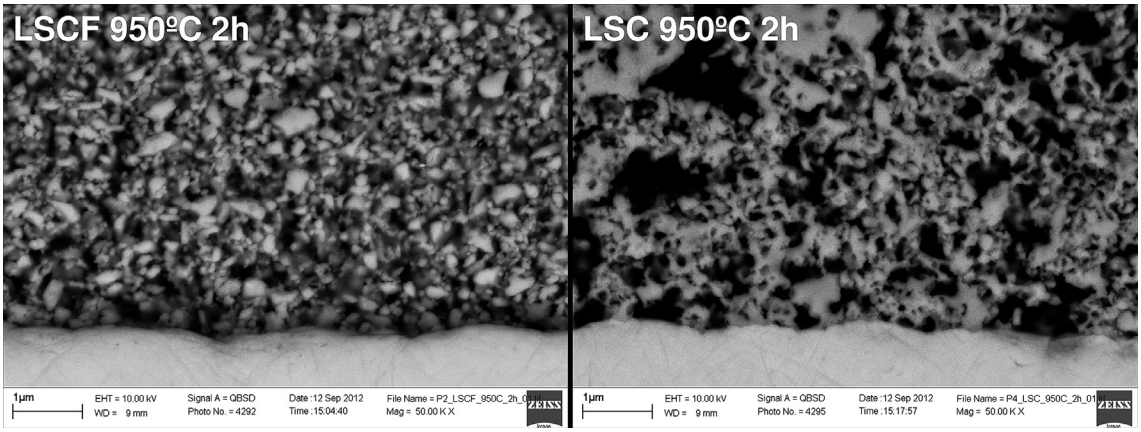

Fig. 11. Cross sectional SEM images of LSCF and LSC cathodes sintered at 950 °C for 2 h.

Eq. (4)) and by the reaction at the MIEC surface (r_r in Eq. (5)). As the sintering temperature T_{max} is increased the grains constituting the cathode grow and the overall surface area decreases, which increases r_r. However, the cathode grain growth and better necking between the individual grains improves the resistance r_{gi}. Thus, r_{gi} decreases while r_r increase with increasing sintering temperature T_{max}. The rate at which these two parameters r_{gi} and r_r change with increasing sintering temperature determines whether the overall Gerischer polarization resistance R_p decrease or increase with increasing sintering temperature T_{max}.

In Fig. 12 the low frequency interception with the real axis of the impedance spectra, which is the total resistance R_t, is plotted as a function of sintering temperature T_{max}. From Fig. 12 it can be observed that R_t decreases with increasing sintering temperature T_{max}. For the LSC and the LSCF cathodes it is possible to observe that a plateau is reached at 800–850 °C, above which a higher sintering temperature does not lower R_t further. This is in contrast to the composite cathodes LSC:CGO and LSCF:CGO where R_t is lowered at each increase in the maximum sintering temperature T_{max}. Analysing the spectra in Fig. 6 it can be seen that for higher sintering temperatures than 850 °C the characteristic skewed semicircle shape of the Gerischer impedance actually increases. It is particular clear for the LSC based cathodes. This can be explained by the decrease in MIEC surface area as the size of the grains constituting the cathode increases. The increase in the Gerischer resistance is compensated by an approximate equivalent decrease in the remaining impedance contributions for the LSC and LSCF cathodes

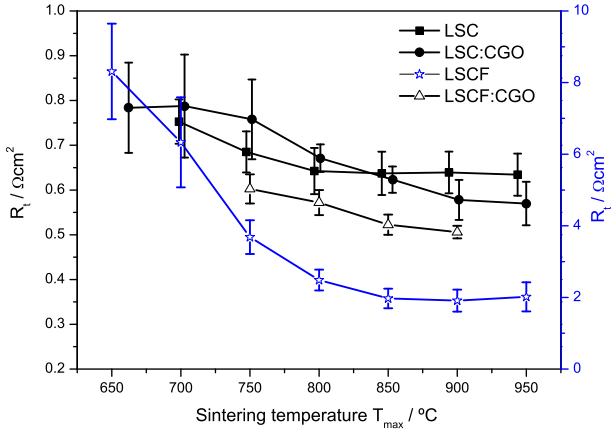

Fig. 12. The total DC resistance R_t determined from impedance spectra as a function of the maximum sintering temperature T_{max}.

and an even greater decrease in the case of the composite LSC:CGO and LSCF:CGO cathodes. A plausible explanation for the observed difference between the single material and the composite cathodes could be the lower sinterability of the CGO phase. Additionally, the CGO particles may act as growth inhibitor for the MIEC particles as it poses a barrier for cation diffusion from one MIEC particles to the next. A need for a higher sintering temperature to sinter the CGO crystallites could explain the results in Fig. 12. In the evaluation of the results in Fig. 12 it is important to remember the effect of a thick 150–300 μm electrolyte which adds to R_s with a relative large constant contribution. In anode or metal supported SOFCs the electrolyte thickness is in the range of 10–15 μm. The impact of a thick electrolyte is that other contributions to R_t may be relatively small and a minimum in R_t as a function of T_{max} is suppressed and appear less significant than it in reality would be in a SOFC.

4.4. Performance as a function of time

The effect of time on the impedance of LSCF, LSC and LSC:CGO cathodes has been studied at the sintering temperatures 750 °C, 800 °C and 850 °C. Common for the evolution of all the cathodes and all the studied sintering temperatures is an improvement with time of the total resistance R_t. Fig. 13 shows representative development of R_t with time at 850 °C. From the figure an exponential like decrease of R_t can be observed. In Fig. 14 the corresponding development of the impedance with time is shown. The inset at the top of Fig. 14 shows the impedance of the LSC:CGO cathode from which it can be seen, that the low frequency gas diffusion contribution has the shape of a Finite-Length-Warburg (FLW) and the magnitude as expected [6,24]. At intermediate frequencies the electrochemical response is located, but due to its small magnitude at 850 °C it is to a large extent overlapped with the response from the gas diffusion and the high frequency arc response originating from the electrolyte grain boundaries. The impedance interpretation has been validated by following the change in the individual EIS arcs as a function of temperature during shut down of the tests. It was found that the given EIS interpretation is in accordance with the spectra of Fig. 6 and the interpretation provided in Section 4.1. Analysis of the spectra in Fig. 4 shows that the improvement with time is a consequence of an improvement in the serial resistance. A similar conclusion can be made for LSCF. For LSC the change with time is first of all very small compared to the changes of LSC:CGO and LSCF. Nonetheless applying the above given interpretation of the LSC:CGO spectra to the LSC spectra it seems that the hf arc changes with time. However, from the inset of Fig. 14 it is possible to argue that the resistance associated with the LSC electrochemical

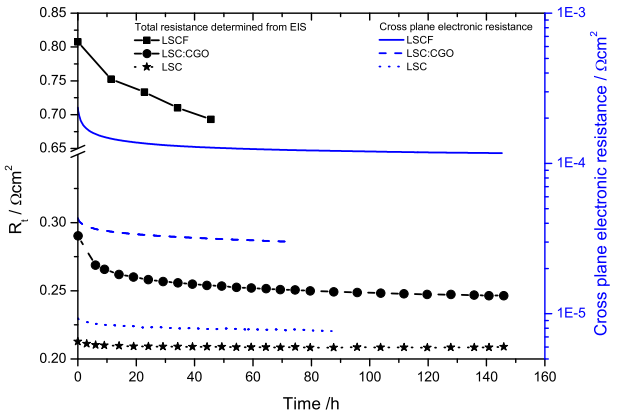

Fig. 13. The effect of sintering time at 850 °C on R_t for LSCF, LSC:CGO and LSC cathodes. For comparison the cross plane area specific electronic resistance of 20 μm thick LSCF, LSC:CGO and LSC cathodes is also included. The cross plane area specific electronic resistance is calculated from the conductivity data in Fig. 2.

Gerischer response has increase with time. An increase in the electrochemical Gerischer impedance contribution will shift the response to lower frequencies reducing the overlap with the hf arc. This could possibly explain the results of a changing hf arc. Given the magnitude of the change and the quality of the impedance spectra it is not meaningful to analyze the observations any further. Alongside the increase of R_t with time in Fig. 13, the evolutions of the cross plane area specific electronic resistance has been included. The cross plane area specific electronic resistance has been calculated on the basis of the experimentally determined in-plane conductivity presented in Fig. 2. From Fig. 13 it is obvious that the magnitude of the cross plane electronic resistance is orders of magnitude lower than R_s. Thus, the electronic conductivity of the cathodes cannot account for the magnitude and the observed change in serial resistances with time. This limits the possible explanations to the current constriction at the cathode/electrolyte interface and hence the adhesion of the cathode to the electrolyte. That there is a long term continues sintering of the cathode is illustrated by the ongoing increase in the electrical conductivity observed in Fig. 2A, where the conductivity increases through the whole measuring period of 85 h for LSC, 75 h for LSC:CGO and 150 h for LSCF. Thus, the evolution in R_s must be due to further sintering, which improves the cathode adhesion and reduces the current constriction at the cathode/electrolyte interface.

5. Overall discussion

The composite cathode SDC:SSC is to our knowledge the best performing cathode sintered at low temperatures reported in the literature [4,25–30]. A polarization resistance R_p ranging from 0.2 to 0.3 Ω cm^2 at 650 °C in air depending on the preparation method has been reported [4]. The SSC:SDC cathode were in these reporting's preferentially sintered in-situ at 800 °C. The LSC and LSC:CGO cathodes in the present study resemble the SSC:SDC cathode to a very high extent. The Sm in the SSC:SDC cathode has essentially been replaced with other similar lanthanoids (La and Gd) in LSC and CGO. Thus, the different cathodes are expected to have some similar properties, e.g. they both show excellent performance and sinterability. However, the LSC and LSC:CGO investigated here had a R_p of around 0.05 Ω cm^2 after sintering at 800 °C (see Fig. 6). This

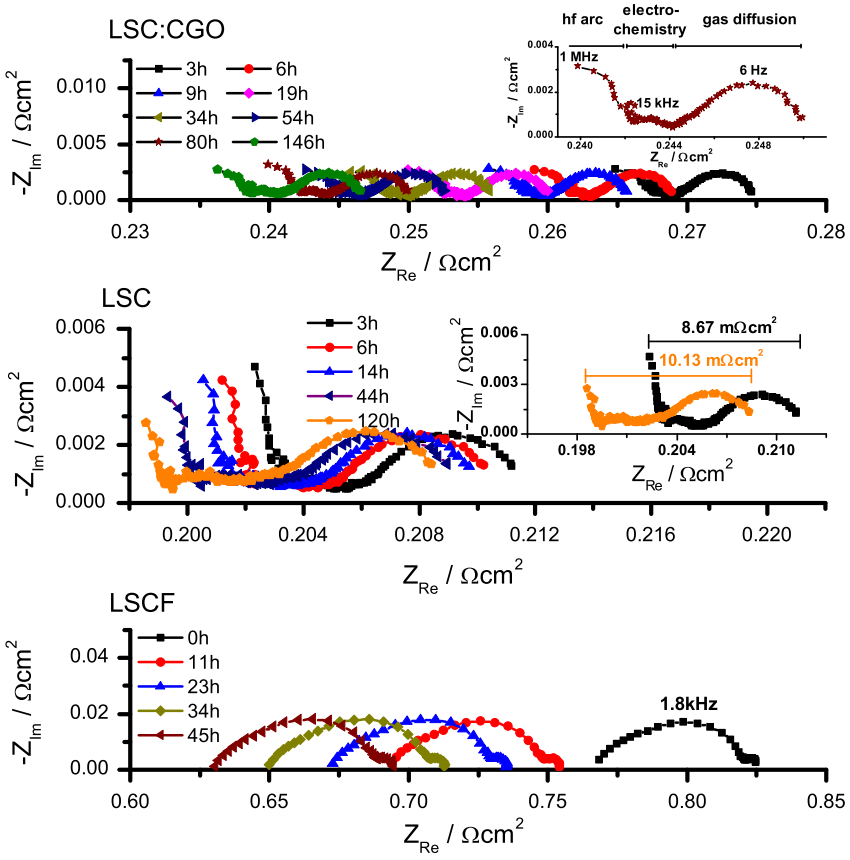

Fig. 14. Representative evolution in impedance of LSCF, LSC:CGO and LSC cathodes the during sintering at 850 °C.

is a factor 4–6 better than the R_p values reported for the SDC:SSC cathodes. It is also clear that LSC and LSC:CGO show similar good adhesion to the electrolyte, and cathode grain connectivity, at relatively low sintering temperatures as the SSC:SDC cathode. In Fig. 10 good adhesion was observed for the LSC:CGO cathodes even after sintering at 750 °C. However, the main drawback of these well-performing and well-sinterable cathodes is a high TEC value of around 18×10^{-6} K^{-1}, where the typical TEC value for the remaining cell components is around 12×10^{-6} K^{-1}. Nonetheless, excellent performance stability was observed for symmetrical cells (with a diameter of 20 mm) with SSC:SDC cathodes during 30 thermal cycling tests in the temperature range 100–600 °C [4]. However, cracks in the SSC:SDC cathode were observed after testing of a MS-SOFC with a cell diameter of 12.7 mm [29] and delamination of the SSC:SDC cathode has also been observed (no information of cell size) [30]. Thus, some discrepancy on the thermal cycling stability of SSC:SDC cathodes seems to exist. As mentioned in the introduction, the mechanical stability of the cathodes depends on numerous parameters, which in principle could explain the apparent discrepancy with respect to thermal cycling stability. Furthermore, large cells should be used for a correct and trustworthy evaluation of thermal cycling stability since long range lateral build-up of stresses is not evaluated on button cell level. If long range lateral build-up of stresses is detrimental to the thermal cycling stability one could consider pattern cathodes. Thus, as mentioned before there are some adjustable parameters to improve the thermal cycling stability.

LSCF has in contrast a reasonable good TEC match with other typical cell components and can be sintered well enough to bond to the electrolyte just below 900 °C (see Figs. 6 and 10), which is desirable for MS-SOFCs. However, the performance is quite poor compared to LSC, LSC:CGO and SSC:SDC cathodes according to the results obtained in Fig. 6. This is in agreement with previous results with LSCF cathodes [5], where an even lower performance for LSCF was observed compared to the present study. MS-SOFCs with in-situ sintered LSCF cathodes have been reported to show moderate performance, but no break down of the losses was provided [2,3].

6. Conclusions

The effect of in-situ cathode sintering temperature and sintering time was systematically studied and compared for LSCF, LSCF:CGO, LSC and LSC:CGO cathodes. From these studies the following conclusions can be drawn:

- In-plane conductivity measurements of the in-situ sintered cathodes showed that LSC, despite a low sintering temperature and the effect of porosity, still shows excellent electronic conductivity with a value of 260 S cm^{-1}. In contrast, LSCF showed a value of 16 S cm^{-1} and indication of significant resistance contributions from poor connectivity of the cathode grains.
- Poor cathode grain connectivity due to insufficient sintering was shown through EIS simulations as a change in the high frequency slope of the characteristic MIEC Gerischer impedance response.
- Poor cathode/electrolyte adhesion was observed for the LSCF cathode as a high frequency arc prior to the EIS Gerischer response.
- SEM investigations of the cathode/electrolyte interfaces of the various cathodes sintered at different temperatures supports the above mentioned EIS conclusions. Furthermore, it was shown that LSC based cathodes are very sintering active even at 750 °C, whereas LSCF requires a significantly higher sintering temperature, at least 850 °C, to achieve sufficient adhesion between the cathode and the electrolyte.
- The cathode/electrolyte adhesion and thus the interfacial current constriction measured as R_s at these low sintering temperatures of 750–850 °C shows an ongoing improvement during very long >75 h sintering times.
- Of the studied cathodes, LSCF showed the lowest performance. In contrast, the low temperature in-situ sintered LSC based cathodes showed excellent performance with a $R_p \sim 0.05$ Ω cm^2 at 650 °C in air.

Acknowledgements

The research leading to these results has received funding from the European Union's Seventh Framework Programme (FP7/2007–2013) for the Fuel Cells and Hydrogen Joint Technology Initiative under grant agreements n° 211940 (METSOFC) and 278257 (METSAPP). Financial support by The Danish National Advanced Technology Foundation, and Energinet.dk under the project ForskEL 2012-1-10806 is also gratefully acknowledged.

References

[1] M.C. Tucker, J. Power Sources 195 (2010) 4570.
[2] Y.M. Park, J.H. Kim, H. Kim, Int. J. Hydrogen Energy 36 (2011) 5617.
[3] N. Oishi, Y. Yoo, Electrochem. Trans. 25 (2009) 739.
[4] D. Lee, I. Jung, S.O. Lee, S.H. Hyun, J.H. Jang, J. Moon, Int. J. Hydrogen Energy 36 (2011) 6875.
[5] S.W. Baek, J. Jeong, Y.M. Kim, J.H. Kim, S. Shin, J. Bae, Solid State Ionics 192 (2011) 387.
[6] J. Nielsen, T. Jacobsen, M. Wandel, Electrochim. Acta 56 (2011) 7963.
[7] Y. Lu, C. Kreller, S.B. Adler, J. Electrochem. Soc. 156 (2009) B513.
[8] J. Bisquert, G. Garcia-Belmonte, F. Fabregat-Santiago, A. Compte, Electrochem. Commun 1 (1999) 429.
[9] J. Bisquert, G. Garcia-Belmonte, F. Fabregat-Santiago, N.S. Ferriols, P. Bogdanoff, E.C. Pereira, J. Phys. Chem. B 104 (2000) 2287.
[10] A. Lasia, M. Schlesinger (Eds.), Modern Aspects of Electrochemistry, vol. 43, Springer, 2009, p. 67.
[11] J. Nielsen, T. Klemensø, P. Blennow, J. Power Sources 219 (2012) 305.
[12] L.J. van der Pauw, Philips Tech. Res. Rep. 13 (1958) 1.
[13] F.W. Poulsen, P. Buitink, B. Malmgren-Hansen, Van der Pauw and Conventional 2-point Conductivity Measurements on YSZ Plates, in: F. Grosz, P. Zegers, S.C. Singhal, O. Yamamoto (Eds.), Proc. 2nd Intl. Symp. on Solid Oxide Fuel Cells (SOFC-II), Athens 1991, Office for Official Publications of the EC, Brussels, 1991.
[14] A. Mineshige, M. Kobune, S. Fujii, Z. Ogumi, M. Inaba, T. Yao, K. Kikuchi, J. Solid State Chem. 142 (1999) 374.
[15] L.W. Tai, M.M. Nasrallah, H.U. Anderson, D.M. Sparlin, S.R. Sehlin, Solid State Ionics 76 (1995) 273.
[16] G.C. Kostogloudis, C. Ftikos, Solid State Ionics 126 (1999) 143.
[17] B.C.H. Steel, Solid State Ionics 129 (2000) 95.
[18] A. Egger, E. Bucher, M. Uang, W. Sitte, Solid State Ionics 225 (2012) 55.
[19] S. Koch, P.V. Hendriksen, Solid State Ionics 168 (2004) 1.
[20] S. Koch, P.V. Hendriksen, T. Jacobsen, L. Bay, Solid State Ionics 176 (2005) 861.
[21] H. Gerischer, Z. Phys. Chem. 198 (1951) 286.
[22] R. de Levie, in: P. Delahay (Ed.), Electrochemical Responses of Porous and Rough Electrodes, Advances in Electrochemistry and Electrochemical Engineering, vol 6, Interscience, New York, 1967, pp. 329–397.
[23] Y.L. Liu, A. Hagen, R. Barfod, M. Chen, H.J. Wang, F.W. Poulsen, P.V. Hendriksen, Solid State Ionics 180 (2009) 1298.
[24] T. Jacobsen, P.V. Hendriksen, S. Koch, Electrochim. Acta 53 (2008) 7500.
[25] R. Hui, D. Yang, Z. Wang, S. Yick, C. Decès-Petit, W. Qua, A. Tuck, R. Maric, D. Ghosh, J. Power Sources 167 (2007) 336.
[26] Y. Xie, R. Neagu, C.-S. Hsu, X. Zhang, C. Decès-Petit, J. Electrochem. Soc. 155 (2008) B407.
[27] Q.-A. Huang, J. Oberste-Berghaus, D. Yang, S. Yick, Z. Wang, B. Wang, R. Hui, J. Power Sources 177 (2008) 339.
[28] R. Hui, J.O. Berghaus, C. Decès-Petit, W. Qu, S. Yick, J.-G. Legoux, C. Moreau, J. Power Sources 191 (2009) 371.
[29] Z. Wang, J. Oberste Berghaus, S. Yick, C. Decès-Petit, W. Qu, R. Hui, R. Maric, D. Ghosh, J. Power Sources 176 (2008) 90.
[30] Q.-A. Huang, B. Wang, W. Qu, H. Rob, J. Power Sources 191 (2009) 297.